IEEE Access
Multidisciplinary | Rapid Review | Open Access Journal

Received October 10, 2020, accepted October 26, 2020, date of publication October 29, 2020, date of current version November 10, 2020.

Digital Object Identifier 10.1109/ACCESS.2020.3034805

Multifunctional Grid-Connected Voltage Source Inverter to Drive Induction Motor Operating With High-Inertia Load

SADJAD MADANZADEH[1], (Graduate Student Member, IEEE), SYED SABIR HUSSAIN BUKHARI[1,2], (Member, IEEE), AND JONG-SUK RO[1]

[1]School of Electrical and Electronics Engineering, Chung-Ang University, Seoul 06974, South Korea
[2]Department of Electrical Engineering, Sukkur IBA University, Sukkur 65200, Pakistan

Corresponding author: Jong-Suk Ro (jongsukro@gmail.com)

This work was supported in part by the Korea Research Fellowship Program funded by the Ministry of Science and ICT through the National Research Foundation of Korea under Grant 2019H1D3A1A01102988, in part by the Basic Science Research Program through the National Research Foundation of Korea funded by the Ministry of Education under Grant 2016R1D1A1B01008058, and in part by the Human Resources Development of the Korea Institute of Energy Technology Evaluation and Planning (KETEP) funded by the Ministry of Trade, Industry and Energy, Korea Government under Grant 20204030200090.

ABSTRACT This paper proposes a novel multifunctional topology for a grid-connected voltage source inverter to control the speed and power flow of a squirrel-cage induction motor. For high-inertia loads during startup, the issues faced include a large transient current and high heat generation. However, the solutions proposed by existing startup methods are inadequate. The topology presented in this study not only addresses the problems related to these methods, i.e., creating a smooth startup, but also presents a flexible alternative for power factor correction using capacitor banks. First, the proposed technique accelerates the motor smoothly to its operating point through the sinusoidal voltage provided by an inverter with an LC filter in its output. In the second step of the control method, after achieving stability in the desired operating point, a converter with an LC filter is assigned the task of power factor correction. Thus, the proposed topology achieves a smooth startup and unity power factor. It includes a new control strategy in which the rotor field-oriented control method is employed for the speed control mode. Finally, the validity of the proposed theory is verified.

INDEX TERMS Field-oriented control, grid-connected inverter, induction motors, power factor correction, startup process.

NOMENCLATURE

Grid:

u	Grid voltage in the bus bar.
v_g, i_g	Grid voltage and current in coupling point.
R_g, L_g	Grid resistance and inductance.
ω_g, f_g	Grid frequency in rad/s and Hz.
θ_g	Voltage phase measured in rad.

Power converter with filter:

v, i	Filter output voltage and current.
v_i, i_i	Inverter output voltage and current.
i_c, i_r	Capacitance and damping resistance currents.
R_f, L_f, C_f	Filter resistance, inductance, and capacitance.
f_r	Resonance frequency.
f_s	Switching frequency.
V_{dc}	DC link voltage.

Motor:

v_s, i_s	Stator voltage and current.
i_{mr}	Rotor-magnetizing current.
R_s, R_r	Stator and rotor resistances.
L_s, L_r, L_m	Stator, rotor and mutual inductances.
σ	Total leakage factor.
τ_r	Rotor time constant.
ω_{mr}, ω_m	Angular speed of the rotor flux vector and rotor.
θ_{mr}, θ_m	Angular position of the rotor flux vector and rotor.
T_e, T_L	Electromagnetic and load torques.

The associate editor coordinating the review of this manuscript and approving it for publication was Meng Huang.

J	Total moment of inertia.
B_m	Coefficient of friction.
n_p	Number of pole pairs.
N_m	Motor nominal speed.
S_n	Motor nominal apparent power.
V_n	Motor nominal voltage.
I_n	Motor nominal current.
f_n	Motor nominal frequency.

Subscripts and superscript in an arbitrary variable x:

x_a, x_b, x_c	Phases in the stationary *abc* frame.
x_d, x_q	Components in the *dq* frame.
x^*	Control reference value.
x^{*1}, x^{*2}	References for control modes 1 and 2.
x_n	Nominal (rated) value.

I. INTRODUCTION

Induction motors (IMs), particularly squirrel-cage induction motors (SQIMs), are interesting for industrial applications as they are compact, economical, and mechanically robust for operation under rush conditions [1]–[3]. These motors can be employed for various loads; however, medium- and high-inertia fan-type loads are the most dominant industrial loads for SQIMs.

The high inertia significantly affects the acceleration time and motor heating. These factors are more critical for IMs, given that, typically, the torque for the first half or more of the torque–speed curve is relatively low, particularly for high-efficiency IMs. Depending on the application and cost, there are several methods for starting three-phase IMs driving high-inertia loads; among them, the most common can be classified into three main categories: full-voltage starting, electromechanical reduced-voltage starting, and solid-state starting [4], [5].

Full-voltage starting is the simplest method as it does not require additional pieces of equipment. During full-voltage (or across-the-line) starting, an IM is connected to the grid through a contactor. Direct across-the-line starting is associated with a large initial current, known as the inrush current, which is typically six to seven times the full load current and is only used if the line disturbances can be tolerated, and the driven load can withstand the shock of an instantaneous application of full voltage to the motor. Although an IM draws the inrush current for a short time, the duration is directly proportional to the load inertia. Thus, for medium- and high-inertia loads, it can result in more severe problems. For instance, the voltage drop at the incoming power connection point resulting from the inrush current can make the network unstable for other grid-connected equipment. A voltage dip and its associated problems will increase in severity if this large current cannot be handled simply in in-plant capacitive buses. Moreover, the inrush current can deteriorate the insulation between the windings by inducing large transitory magnetic forces in the stator windings, forcing the windings to move and distort from their actual position. During acceleration, the temperature rises rapidly within both, the rotor and stator. As a result, a higher heat level due to a prolonged startup time associated with high-inertia loads can cause serious problems, particularly for the winding insulation; hence, it may not be possible to start the motor again until it cools [4], [6].

Electromechanical reduced-voltage starting has been in existence nearly as long as the IM itself. Auto-transformer starting, wye-delta (star-delta) starting, and resistor/reactor starting can be referred to as electromechanical reduced-voltage starting methods, which can be implemented using a mechanical switch or contact. These methods allow for the limiting of the transient current peak. By considering factors such as core saturation and skin effect, a reasonable linear reduction for the drawn current can be expected with decreasing voltage. However, these methods still present some challenges; auto-transformer starting, for example, causes a current spike at the transient instant and the resultant transient torque may cause problems for the driven equipment. Moreover, this method is more expensive than both wye-delta and resistor/reactor starting. On the other hand, overload protection for both the wye and delta connections and additional contactors are some of the issues associated with wye-delta starting. In a series-connected element, there are problems such as the wastage of energy as heat in the resistor and torque pulsations while switching the resistor or reactor out of the circuit [7], [8].

Solid-state starters, introduced in the early 1970s, led to the development of electronic soft starters as well as inverter-controlled variable frequency drive (VFD) starters. These devices employ programmable logic controllers in combination with sophisticated power electronic circuits to provide a smooth start. Electronic soft-starting techniques can be classified into voltage ramp starting and current limit starting methods. Voltage ramp starting progressively increases the voltage supplied to the motor through control of the firing angle of the switches (SCRs) [9]–[11]. Although voltage ramps have a simple form, the voltage harmonics associated with this method contribute to additional resistance losses in IMs, while only the fundamental harmonic of the voltage creates the working torque. In current limit starting, the user can set a predefined maximum current that will be supplied to the motor. However, similar to electromechanical starting, the disadvantage associated with this type of starting is a reduction in torque resulting from a reduction in current. VFDs control an IM such that it operates on the right side of the breakdown on the speed–torque curve at a low slip (near-synchronous speed) through supplying a variable frequency voltage. Using this method, a high torque can be achieved across the entire speed range, implying that the motor can rotate the load as slowly as desired and maintain maximum torque. Its other advantages include eliminating the mechanical stress and inrush current. As rotor losses are associated with slip speed, a significant reduction in rotor losses, and consequently, relatively little rotor heating during startup is observed using VFD starting, and the problem of

thermal stress (overheating) is not experienced. VFD offers maximum control over the starting characteristic for any load type. However, this method is considerably more expensive than the other techniques discussed above and takes up more space than other electronic soft starters. In addition, VFD starting results in a relatively long acceleration time because the maximum drive currents and accordance torque are typically 150–200% of their full load values. If faster acceleration times are desired, the drive must be suitable for supplying higher current during the startup period [12]–[14].

On the other hand, as existing motors are usually not designed for inverter supply, feeding an SQIM through a pulse-width-modulated voltage source inverter (VSI) subjects it to voltage and current surges. This can result in several issues, such as additional losses in the motor, insulation failure, high bearing current, and electromagnetic interference. As a solution, an LC filter can be employed between the VSI and the motor to create sinusoidal output voltages and provide conditions for the machine similar to those for the grid operation [15].

Clearly, all the methods described above present some problems; moreover, after starting, the employed starting equipment does not have any use in motor operation. Although VFD is the most efficient method, it is expensive, particularly when used with an LC filter to provide sinusoidal voltage to feed the motor.

Therefore, this study proposes a multifunctional technique for driving an IM with high-inertia load. We selected an SQIM as it is the most popular IM in a wide range of industrial applications. Although an SQIM has been considered as the case study in this paper, the proposed theory can be extended to other types of single- and three-phase motors, including rotor-wounded IM. This study involves an inverter with an LC filter to drive high-inertia loads. However, using an inverter for only the purpose of starting a high-inertia load can be expensive. Therefore, using the proposed multifunctional topology, once the motor reaches a steady-state running condition, the inverter can be used to supply reactive power to the IM. Thus, the power factor can be significantly improved, and the cost that utilities often charge for a lagging power factor load because of the additional losses in the feeding transformer and distribution line can be eliminated. In the proposed theory, the inverter not only resolves the problem of motor heating and helps adjust the machine torque, but also injects the required reactive power to achieve a unity power factor.

The proposed method offers a cost-effective solution to improve startup and power factor features. It has been mentioned as a cost-effective technique because, generally, when an inverter serves as a soft-starter, it goes out of the circuit after completing the startup process. It means it does not participate efficiently in the whole motor operation. Besides, bank capacitors include several capacitors so that some can be assigned to correct the power factor when it changes for different loads. It also means that all capacitors are not always in the circuit. Providing several capacitors in high powers and replacing the broken ones cost a lot, while these capacitors only provide a unity power factor for a few discrete loads.

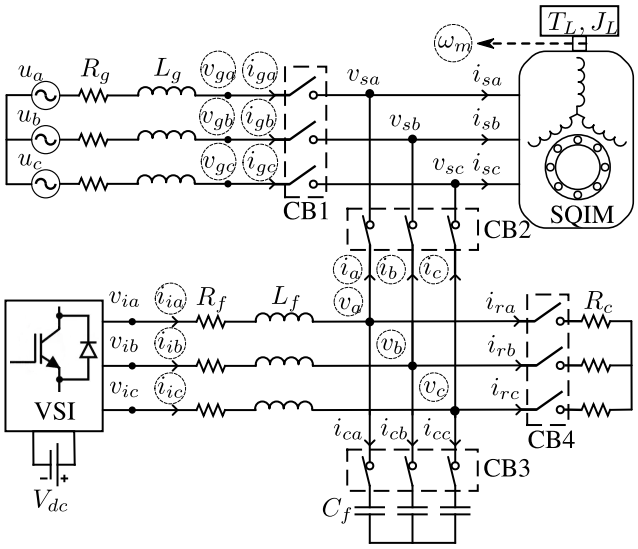

FIGURE 1. Proposed scheme of multifunctional grid-connected voltage source inverter to drive induction motor with high-Inertia Load.

In contrast, for the provided topology, the inverter participates in the whole motor operation. Also, only one capacitor bank as a filter is used in the system. This capacitor is smaller than the general capacitor banks used for power factor correction because it is not required to provide all reactive power. Moreover, this topology provides a continuous range of reactive power injection proper for different loads.

The rest of this paper is organized as follows. Section II presents the novel topology to resolve the startup and power factor issues. Section III describes the proposed control system to control the speed and power flow. Section IV presents the detailed verification results for both steady-state and transient response of the SQIM for speed control and power flow control modes, and demonstrates the effectiveness of the proposed topology and its associated control technique. The conclusion of this paper, including a summary of the main points, is presented in Section V.

II. PROPOSED MULTIFUNCTIONAL TOPOLOGY TO CONTROL SPEED AND POWER FLOW

IMs are used in most industrial applications because they are compact and economical. In such applications, IMs are often integrated with heavy mechanical loads. This section provides a better alternative for the challenges encountered in starting high-inertia loads. In addition to the methods described in the previous section to start up IMs, another solution employed by manufacturers is the use of a double-cage induction motor to produce extra starting torque. However, the torque of the machine under such a condition is not adjustable; one of the problems addressed by the proposed topology is shown in Fig. 1.

Fig. 1 shows a simplified diagram of the proposed multifunctional topology. According to this scheme, by using an inverter, the starting problem of the induction machine can

be resolved. In the first operating state, when the system is disconnected from the grid (offline mode), switches CB2 and CB3 are closed, while CB1 and CB4 are open; CB4 is to connect the auxiliary resistance bank. This operating state aims to control the motor speed in such a way that the motor accelerates while maintaining the torque, current, and voltage within a safe limit; it can then provide a safe connection condition to connect to the grid (online mode) through a synchroscope. However, the usage of the inverter solely for starting the induction machine would be costly. Hence, the inverter can serve to improve the power factor of the system during the steady-state operation in the online mode (connected to the grid) because of its capability of providing reactive power. Under such a condition, the inverter will keep powering the induction machine with balanced input voltages and currents. Thus, in the second operating state, CB1, CB2, and CB3 are closed, while CB4 is open, so that the grid provides the required active power and the inverter injects the reactive power.

It should be noted that the encircled symbols in Fig. 1 indicate the electric and mechanical variables requiring measurement for the control system.

III. PROPOSED SPEED AND POWER FLOW CONTROL

As mentioned above, the proposed algorithm involves online and offline operating modes. The first mode involves speed control (Step 1), and subsequently, the online mode controls the power flows (Step 2) when the motor is fed through the grid. A simple diagram of the control algorithm is shown in Fig. 2. In Step 1, the SQIM is started up and accelerated to reach its nominal speed and torque. Step 2 of the control algorithm starts when the motor is stabilized at its desired operating point and connected to the grid during a safe connection procedure. Next, in Step 2, the SQIM is fed by the grid, while the inverter is controlled to inject a desired current to keep the power factor of the grid as unity. The two steps create voltage references to command a VSI, as shown in Fig. 2, where CM is the signal of the control mode to command for switching between modes.

The control system involves transferring the system variables from the stationary *abc* frame to the *dq* frame. It also adops an active damping (AD) technique to suppress the resonant harmonics described below.

A. DESCRIPTION OF THE SYSTEM MODEL

The studied system is a three-phase two-level VSI-fed 15 kVA, 400 V, 21.7 A, 4-pole, 50 Hz, 1475 r/min, 3-phase, star-connected SQIM with 3-phase second-order low-pass sinusoidal LC filter. The system parameters are detailed in Table 1, and the nomenclature used is shown on the first page.

The control algorithm is based on the system model in the *dq* reference frame. In what follows, the mathematical models of both SQIM and LC filters are derived through Park and Clark transformations.

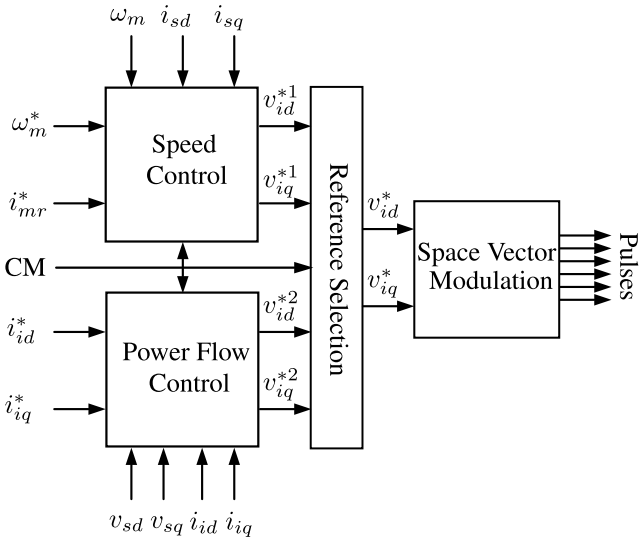

FIGURE 2. Block diagram of speed and power flow control modes.

1) MATHEMATICAL MODEL OF SQIM

The dynamic behavior of an induction machine can be described in rotor field coordinates by the following equations, where the effects of the core and eddy current losses have not been accounted for [16]:

$$v_{sd} = R_s i_{sd} + \sigma L_s \frac{di_{sd}}{dt} - \sigma L_s \omega_{mr} i_{sq} + (1-\sigma) L_s \frac{di_{mr}}{dt}, \tag{1}$$

$$v_{sq} = R_s i_{sq} + \sigma L_s \frac{di_{sq}}{dt} + \sigma L_s \omega_{mr} i_{sd} + (1-\sigma) L_s \omega_{mr} i_{mr}, \tag{2}$$

$$i_{sd} = i_{mr} + \tau_r \frac{di_{mr}}{dt}, \tag{3}$$

$$\omega_{mr} = \frac{1}{\tau_r}\left(\frac{i_{sq}}{i_{mr}}\right) + n_p \omega_m, \tag{4}$$

where $\sigma = 1 - L_m^2/(L_s L_r)$ and $\tau_r = L_r/R_r$. The equation of motion is

$$J\frac{d\omega_m}{dt} = T_e - B_m \omega_m - T_L. \tag{5}$$

2) MATHEMATICAL MODEL OF LC FILTER

In the *dq* frame, the differential equations of the LC filter can be presented as the following inductor current equations [16]:

$$v_{id} = R_f i_{id} + L_f \frac{di_{id}}{dt} - L_f \omega i_{iq} + v_{sd}, \tag{6}$$

$$v_{iq} = R_f i_{iq} + L_f \frac{di_{iq}}{dt} + L_f \omega i_{id} + v_{sq}, \tag{7}$$

and the capacitor voltage equations can be presented as follows.

$$i_{id} = C_f \frac{dv_{sd}}{dt} - C_f \omega v_{sq} + i_{sd} \tag{8}$$

$$i_{iq} = C_f \frac{dv_{sq}}{dt} + C_f \omega v_{sd} + i_{sq} \tag{9}$$

In the offline control mode, where the d-axis is oriented in the direction of the rotor flux, $\theta = \theta_{mr}$ is used for dq transformation, while in the online control mode, the angular position of the reference frame is $\theta = \theta_g$ to control the system based on the phase and frequency of the grid voltage. Thus, in (6)–(9), ω for the offline and online modes is indicated as ω_{mr} and ω_g, respectively.

3) CALCULATION OF FILTER PARAMETERS

According to the method proposed in [17] and [18], which forms the base of the LC filter design in this study, the resonance frequency of the system should be in the range between ten times the rated frequency (10×50 Hz $= 500$ Hz) of the motor and one-third of the inverter switching frequency ($5000/3$ Hz $= 1666$ Hz). The inverter switching frequency that is acceptable for thermal reasons lies only slightly above the resonance frequency of the LC filter. However, it causes problems related to dynamic stator current control.

The selection of L_f is a tradeoff between the inductor current ripple amplitude and inductor size. The filter inductance is chosen such that the voltage drop across the filter inductor and inverter current ripple can meet the following two criteria. First, the voltage drop calculated from (10) should not exceed the allowable value of 10% of the rated phase voltage of the motor ($400/\sqrt{3}$ V) at the rated frequency and current of the motor (50 Hz and 10 A). Second, the current ripple defined as (11) must be within 15–25% of the peak value of the rated inductor current; in this case, the nominal value of the inverter current is assumed to be equal to I_n.

$$v_L = i_i\sqrt{R_f^2 + (2\pi f_n L_f)^2} \tag{10}$$

$$\Delta i_i = \frac{V_{dc}}{8 f_s L_f} \tag{11}$$

The capacitor value is determined such that the resonance frequency of the system f_r calculated based on (12) meets its constraints. There is a tradeoff between the filter size and attenuation of the resonance frequency by the control action.

$$f_r = \frac{1}{2\pi\sqrt{L_{eq}C_f}} \tag{12}$$

where the equivalent inductance L_{eq} derived by the Thevenin equivalent circuit of the motor and filter can be obtained as follows.

$$L_{eq} = \frac{L_f(L_{ls} + L_{lr})}{L_f + L_{ls} + L_{lr}} \tag{13}$$

B. ROTOR FIELD-ORIENTED CONTROL FOR VSI-FED SQIM WITH LC FILTER (OFFLINE MODE)

This study employs an active damping-based RFOC for a SQIM with an LC filter for the offline mode when the system is fed using a VSI only. Fig. 3 shows a scheme of the block diagram of the speed control mode (offline state) [19].

The RFOC system for a SQIM is often used in adjustable speed drives of the IM. This closed-loop cascade control technique is developed based on the motor equations expressed in a synchronously rotating dq reference frame aligned with the rotor flux vector. In Step 1, as Fig. 3 shows, speed control is performed to accelerate and stabilize the motor to its nominal operating point through the outer loop of the cascade structure, when the rotor field is controlled by applying the reference rotor-magnetizing current. The output of the speed PI controller, i^*_{sq}, is used to provide the required electromagnetic torque to track the reference speed. Instead of providing the d and q reference currents, as shown in Fig. 3, an alternative solution is to adopt the maximum torque per ampere (MTPA) strategy in the speed control mode [20], [21]. This strategy can be used to obtain optimum current references to minimize the heat generated due to the resistance losses. MTPA can provide the desired torque using a minimum current during the accelerating time and before connecting to the grid, to minimize the resistance losses. As shown in Fig. 3, after decoupling the reference stator voltage components by adding the decoupling terms, e_{sd} and e_{sq}, given as

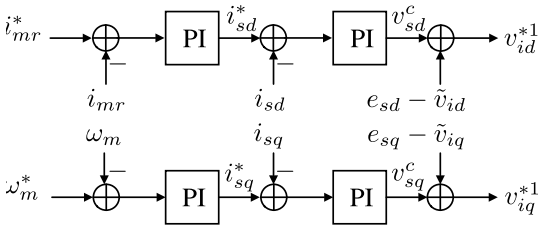

FIGURE 3. Block diagram of the speed control mode.

$$e_{sd} = -\sigma L_s \omega_{mr} i_{sq} + (1-\sigma)L_s \frac{di_{mr}}{dt}, \tag{14}$$

$$e_{sq} = \sigma L_s \omega_{mr} i_{sd} + (1-\sigma)L_s \omega_{mr} i_{mr}, \tag{15}$$

the resultant signals must be passed through a damping process to generate the inverter voltage references. Applying v^c_d and v^c_q directly to the space vector modulation block results in high-magnitude resonance oscillations in the stator voltage and current. The proposed control algorithm, in the whole offline mode, adopts an efficient current-based active damping technique to damp out the resonance frequency oscillations and to stabilize the unstable operating point added by the LC filter to the closed-loop system through the generation of $\tilde{v}_{id}$ and $\tilde{v}_{iq}$ signals for the current control loops (Fig. 3). Besides offering simplicity, this damping method does not require retuning of the controllers of the conventional RFOC without an LC filter.

The general equation of the electromagnetic torque in a synchronous dq reference frame is given as

$$T_e = \frac{3}{2} n_p(\lambda_{sd} i_{sq} - \lambda_{sq} i_{sd}). \tag{16}$$

However, in the rotor flux reference frame, where the q component of the rotor flux λ_{qr} equals zero, (6) can be rewritten as follows [20].

$$T_e = \frac{3}{2} n_p (1-\sigma) L_s i_{mr} i_{sq} \tag{17}$$

In the steady state, $(d/dt = 0)$, $i_{mr} = i_{ds}$, and thus, the electromagnetic torque equation can be given as

$$T_e = \frac{3}{2} n_p (1-\sigma) L_s i_{sd} i_{sq}. \tag{18}$$

Referring to (5) and (17), the inverter must have the capability to provide the current needed to generate the required electromagnetic torque to accelerate the motor to its operating speed.

The motor must reach its nominal operating point before reaching its voltage limitation. Due to the DC link voltage, the VSI has limitations in generating its terminal voltages. Omitting the possible overmodulation, the maximum inverter output voltage $V_{i,\max}$, defined in (19), is $V_{dc}/\sqrt{3}$.

$$v_{id}^2 + v_{iq}^2 \le V_{i,\max}^2 \tag{19}$$

1) ACTIVE DAMPING TECHNIQUE

Similar to RFOC, the equation of the adopted AD technique is formulated using dq variables in the rotor flux reference frame. To implement the AD technique, the d and q components of the inverter currents are first passed through a low-pass filter to extract the dc component $\bar{i}_{ix}$, and then the high-frequency components are obtained as (18).

$$\tilde{i}_{ix} = i_{ix} - \bar{i}_{ix}, x = \{d, q\} \tag{20}$$

Next, the compensating voltage signals can be constituted from (21). This method damps out the oscillations in the resonance frequency and stabilizes the unstable operating point by subtracting these components from the stator reference voltage signals (Fig. 3).

$$\tilde{v}_{ix} = K_{damp} \tilde{i}_{ix}, x = \{d, q\} \tag{21}$$

The adopted AD is based on shifting the poles and zeros of the unstable operating points of the closed-loop drive to shift in the left-half s-plane. Thus, the damping coefficient must be appropriately selected to meet this goal [22]. This study uses the method presented in [19] to design the AD method and select K_{damp}.

It is possible to connect a proper value of resistance in series with the capacitor to replace the system's poles in a proper position of the s-plane and make the system stable. Resistance can be connected in series with the capacitor to damp out the LC resonance. However, this solution increases power loss in the system. An AD method can be used to achieve lossless damping. In this way, a fictitious resistance value is multiplied by the individual capacitor currents at the resonant frequency and subtracted from the source voltages. Thus, a damping effect of the resistance is emulated but in a lossless manner.

C. POWER FACTOR CORRECTION (ONLINE MODE)

When both inverter and grid are synchronized through a phase-locked loop before switching to the grid, and the SQIM stabilizes at its operating point, Step 2 begins, in which speed control through RFOC is not involved. In the proposed multifunctional topology shown in Fig. 1, the VSI is connected to a three-phase grid through an inductance working as a filter. In this study, the grid resistance and inductance, R_g and L_g, are assumed to be zero, and a balanced state of the grid is assumed. To design a control system for power factor correction, the three-phase model of the AC side of the inverter system can be expressed in the rotating reference frame synchronized with the grid voltage using the Park transformation, such as (6) and (7), when $\omega = \omega_g$.

In industries, where most load is inductive load because of the use of electric motors, capacitor banks are utilized to correct the power factor to near unity. The capacitors are switched in and out through mechanical contactors. However, because these contactors are relatively slow, they cannot react to sudden momentary dips in voltage, commonly observed in a weak grid, and can add significant stress to the utility grid [23]. In addition, these capacitance banks are designed to provide a unity power factor only in a few specific loads. A multifunctional VSI is proposed here as a dynamic volt ampere reactive (VAR) compensator system. Through this topology, the required reactive power is calculated, and then instantaneously compensated by injecting leading or lagging reactive power at the common point with the grid. Through the VAR control system, reactive power is supplied to the network within a fraction of a second. The control system computes the amount of active and reactive power needed in the synchronous frame, given by

$$P = v_d i_d + v_q i_q, \tag{22}$$

$$Q = v_q i_d - v_d i_q. \tag{23}$$

The basic principle of the adopted method is to control the instantaneous active and reactive grid currents, and consequently, the active and reactive power through separate controllers that are independent of each other. The grid voltages and currents are first sensed, and through a phase-locked loop (PLL), the grid phase angle and frequency are detected. The amount of power required is first estimated from the utility grid at the desired power factor; this allows the reference currents in a synchronous frame synchronized with the grid voltage to be calculated. Consequently, the current controllers attempt to bring the actual currents to their references [24].

The reference currents i_{id}^* and i_{iq}^* can be calculated from the power equations (22) and (23), such that

$$i_{id}^* = \frac{v_{sd} P_i^* + v_{sq} Q_i^*}{v_{sd}^2 + v_{sq}^2}, \tag{24}$$

$$i_{iq}^* = \frac{v_{sq} P_i^* + v_{sd} Q_i^*}{v_{sd}^2 + v_{sq}^2}. \tag{25}$$

Assuming zero active power command and given that in the grid reference frame, $v_{sq} = 0$, the current command equations can be obtained as

$$i_{id}^* = 0, \tag{26}$$

$$i_{iq}^* = \frac{Q_i^*}{v_{sd}}. \tag{27}$$

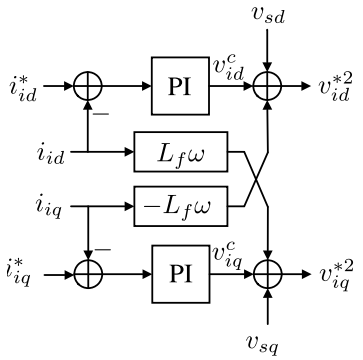

FIGURE 4. Block diagram of the power flow control mode.

To provide all reactive power using a VSI, capacitance Q_i^* in (27) can be calculated as follows.

$$Q_i = Q_s + Q_c = v_{sd} i_{sq} - v_{sd}^2 C_f \omega \tag{28}$$

Although it is not the most accurate method for calculating the reference reactive power due to variations in filter capacitance, it is the simplest one. As shown in Fig. 4, by canceling the effect of the coupling term between the d-axis and q-axis, the PI current controllers can be employed to generate controller voltages v_{id}^c and v_{iq}^c, and then form the inverter reference voltages, as follows.

$$v_{id}^* = v_{id}^c + v_{sd} - L_f \omega i_{iq} \tag{29}$$
$$v_{iq}^* = v_{iq}^c + v_{sq} + L_f \omega i_{id} \tag{30}$$

The steady-state model of SQIM in the grid frame (stator synchronous reference frame) can be expressed as [24]

$$v_{sd} = R_s i_{sd} - \omega_g L_s i_{sq} - \omega_g L_m i_{rq}, \tag{31}$$
$$v_{sq} = R_s i_{sq} + \omega_g L_s i_{sd} + \omega_g L_m i_{rd}, \tag{32}$$
$$0 = R_r i_{sd} - \omega_{slip} L_m i_{sq} - \omega_{slip} L_r i_{rq}, \tag{33}$$
$$0 = R_r i_{sq} + \omega_{slip} L_m i_{sd} + \omega_{slip} L_r i_{rd}. \tag{34}$$

Solving these equations for the current components, and then substituting the obtained values in the steady-state form of LC filter equations, derived from (6)–(9), the voltage limitation $V_{i,\max}$ and minimum DC voltage can be calculated, as will be described in Section IV.

IV. RESULTS AND DISCUSSION

Considering the values of voltage drop, current ripple, and resonance frequency as 14.5 V (6.3%), 7.4 A (24%), and 790 Hz, respectively, the per-phase filter parameters, L_f and C_f, can be calculated, as listed in Table 1.

For the studied SQIM with parameters listed in Table 1, from (5), the required torque was calculated as 145 Nm when the motor was close to its operating point with an acceleration of 590 r/s^2. With a magnetization current of 19.1 A, under the steady-state condition, and using (18), the dq component of the current can be calculated to generate the required torque. The inverter voltage components can now be derived from (1) to (4) and (6) to (9) in the steady state ($d/dt = 0$).

TABLE 1. Parameters of the studied system.

	Parameter	Value
Inverter	R_f	0.12 Ω
	L_f	2.1 mH
	C_f	40 μF
	f_r	790 Hz
	f_s	5000 Hz
	V_{dc}	620 V
Motor	S_n	15 kVA
	V_n	400 V
	I_n	21.7 A
	R_s	0.2 Ω
	R_r	0.22 Ω
	L_s	53.5 mH
	L_r	53.5 mH
	L_m	52.6 mH
	J	1.2 kg.m^2
	B_m	0.0092 Nm.s/rad
	n_p	2 pairs
	N_m	1475 r/min
	T_L	69.5 Nm

These values were obtained as $v_{id} = -26.3$ V and $v_{iq} = 327.8$ V. Therefore, the voltage limitation $V_{i,\max}$ defined as (19) was calculated as 351.1 V, where a minimum DC voltage of 608.2 V was required in the speed control mode.

For the power control mode, by solving equations (31)–(34) for the current components when $v_{sd} = 400/\sqrt{3}$ V, $v_{sq} = 0$ V, and the slip speed $\omega_{slip} = \omega_g - n_p\omega_m$, the current components of the stator were obtained as $i_{sd} = 8.5$ A and $i_{sq} = -13.7$ A. Substituting these values in the steady-state form of LC filter equations derived from (6) to (9), and applying the same method as that explained for the speed control mode, the voltage limitation $V_{i,\max}$ was calculated as 138 V and the minimum DC voltage as 239.1 V. The DC voltage must be considered as the maximum value between 608.2 and 239.1 V. Thus, the DC link voltage was taken to be 620 V, based on the maximum value of the voltage calculated for the speed and power control modes.

The required DC link can be provided using a rectifier. However, as it is not the main focus of this study, the DC link has been modeled using a battery.

Two scenarios were applied to the motor to examine the proposed theory: a) startup through a direct connection to the network and b) startup and power factor correction using multifunctional topology.

The reference magnetizing current was $i_{mr}^* = 19.1$ A and it was applied at $t = 0$ s. The reference speed was $\omega_m^* = 1475$ rpm, applied at $t = 0.5$ s, when the magnetizing current was stabilized at its desired value. The reference speed was applied as a ramp function; the reference speed rose from 0 to 1475 rpm (acceleration of 590 r/s^2) in 2.5 s. In addition, the fan load reached a value of 69.5 Nm at the nominal speed.

Fig. 5 shows the motor speed achieved in the mentioned scenarios. Clearly, if the motor constraints, including the winding and mechanical constraints, allow a direct connection to the grid, it can accelerate the motor faster to the desired speed. However, the gradual speed increase achieved through

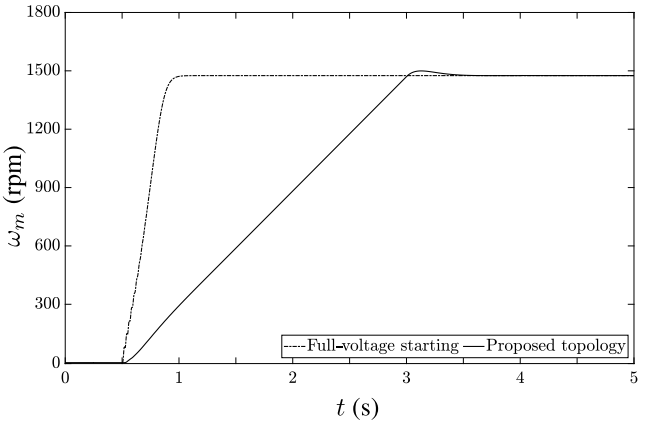

FIGURE 5. Mechanical speed of the motor.

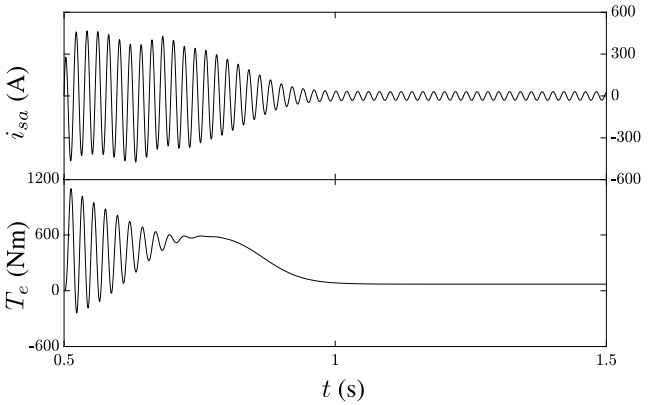

FIGURE 6. Stator phase current and electromagnetic torque (full-voltage starting).

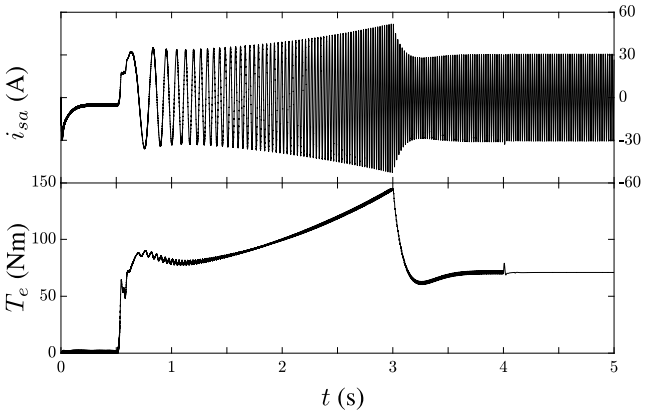

FIGURE 7. Stator phase current and electromagnetic torque (proposed topology).

the proposed topology in the speed control mode results in maintenance of the electromagnetic torque and current within their safe constraints (Figs. 6 and 7). It also avoids intense heat generation, especially for high-inertia loads, where the starting time is longer. In addition, as fast speed-tracking is not usually as important as a safe startup in the aimed applications of this paper, a reasonably longer startup time would not be considered an issue.

When the motor reached its operating speed, and after synchronization with the offline system, it was switched to

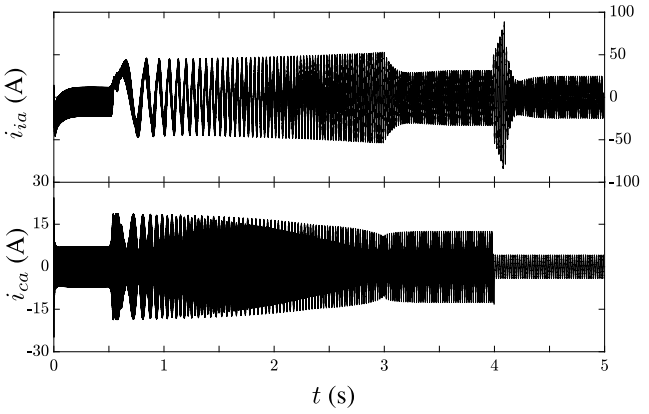

FIGURE 8. Inverter phase current and capacitance phase current (proposed topology).

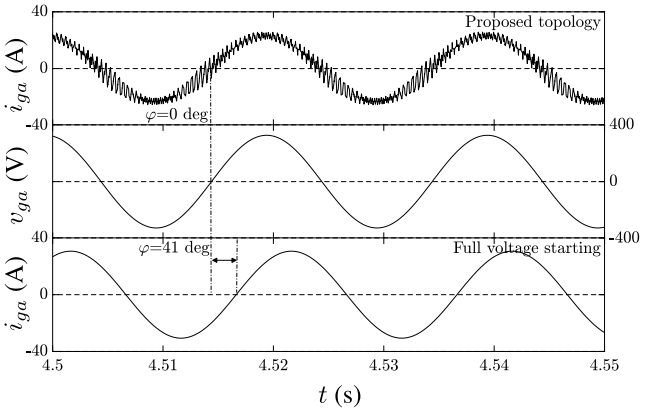

FIGURE 9. Grid voltage in coupling point and grid current (the nominal load).

the grid at s. Fig. 5 shows that when the motor connects to the network and when the voltage in the stator terminals is synchronous with the grid, it keeps rotating at its nominal speed. In addition, Fig. 7 shows that the studied SQIM draws the same current and generates the same electromagnetic torque in the online mode. However, the current injected by the VSI changes based on the desired reference current components in the power flow control mode. After going through the transient state, the steady-state current has a lower magnitude compared to the speed control mode, because in the online mode, the inverter only injects the current contributing to the reactive power, and active power is provided through the grid. This causes the current drawn from the grid to have the same phase as its voltage, as shown in Fig. 9. In contrast, when the SQIM is only fed through the grid, there is a 41° phase lag between the current and voltage. Due to the nature of capacitance, the current is related to the voltage derivation. Smaller ripples in the voltage cause smaller ripples in the capacitor phase current when the capacitor is connected to the grid (Fig. 8). As shown in Fig. 8, there is an increase in the inverter current after switching to the grid. It is an overshoot on inverter current when it tracks the step reference to achieve the unity power factor. While designing the

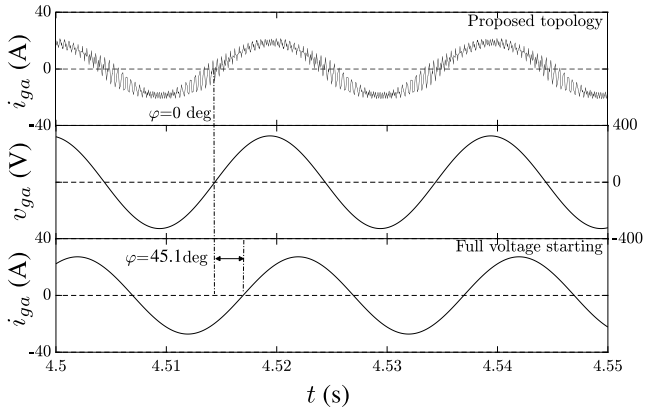

FIGURE 10. Grid voltage in coupling point and grid current (80% of the nominal load).

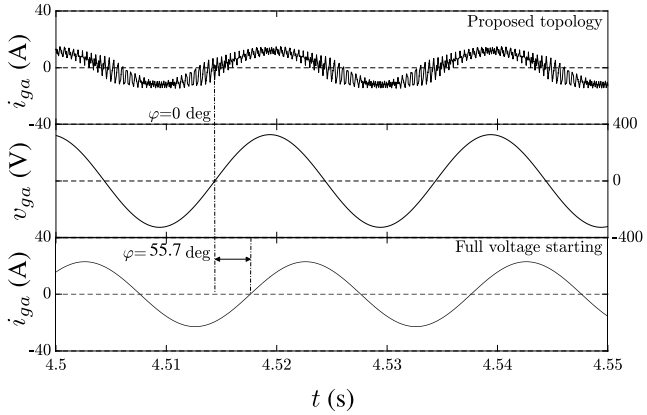

FIGURE 11. Grid voltage in coupling point and grid current (50% of the nominal load).

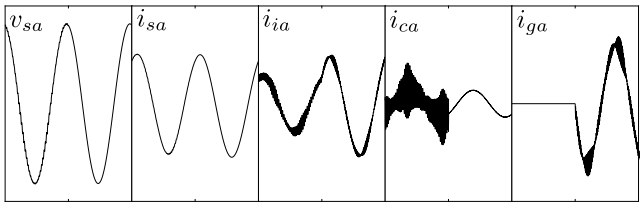

FIGURE 12. Magnified phase current and voltage while connecting to the grid.

current controllers in Fig. 4, the overshoot must not exceed the current constraint of the inverter.

Same as Fig. 9, Figs. 10 and 11 show the grid voltage and currents for both startup methods when the motor operates with 80% and 50% of its nominal load. These figures verify that the proposed topology can continuously inject the proper amount of reactive power to achieve a unity power factor for all range of loads without requiring several capacitor banks for different loads.

Fig. 12 provides a horizontally magnified view of the voltage and currents from $t = 3.98$ s to $t = 4.02$ s showing the detailed changes when the mode is changed from offline to online (for full load operating condition).

V. CONCLUSION

This study proposed a new multifunctional topology that achieves a smooth startup and unity power factor. The proposed topology implemented using a VSI and an LC filter solved the problems related to previous startup methods and at the same time injected reactive power to correct the power factor when the motor was fed through the grid. The proposed topology was associated with a new control strategy covering both speed and power flow control modes. The investigation of the proposed topology confirmed that it can decrease the heat generation, particularly for high-inertia loads, by controlling the starting current. In addition, the proposed topology offers the potential benefit of using the LC filter and VSI to correct the power factor in the online mode, making this topology an optimum solution in terms of cost for such applications.

REFERENCES

[1] M. Manohar and S. Das, "Current sensor fault-tolerant control for direct torque control of induction motor drive using flux-linkage observer," *IEEE Trans. Ind. Informat.*, vol. 13, no. 6, pp. 2824–2833, Dec. 2017.

[2] X. Shi and M. Krishnamurthy, "Digital control of induction machines as a backup control strategy for fault tolerant operation of traction motors," *IEEE J. Emerg. Sel. Topics Power Electron.*, vol. 2, no. 3, pp. 651–658, Sep. 2014.

[3] I. Sami, S. Ullah, Z. Ali, N. Ullah, and J.-S. Ro, "A super twisting fractional order terminal sliding mode control for DFIG-based wind energy conversion system," *Energies*, vol. 13, no. 9, p. 2158, May 2020.

[4] R. F. McElveen and M. K. Toney, "Starting high-inertia loads," *IEEE Trans. Ind. Appl.*, vol. 37, no. 1, pp. 137–144, Jan. 2001.

[5] A. Eliasen, "High-inertia drive motors and their starting characteristics," *IEEE Trans. Power App. Syst.*, vols. PAS–99, no. 4, pp. 1472–1482, Jul. 1980.

[6] M. Melfi and S. Umans, "Squirrel-cage induction motors: Understanding starting transients," *IEEE Ind. Appl. Mag.*, vol. 18, no. 6, pp. 28–36, Nov. 2012.

[7] J. Yuan, C. Wang, Y. Zhu, and B. Chen, "A novel soft start method of super large capacity high voltage motor," *CES Trans. Electr. Mach. Syst.*, vol. 3, no. 3, pp. 302–308, Sep. 2019.

[8] F. M. Bruce, R. J. Graefe, A. Lutz, and M. D. Panlener, "Reduced-voltage starting of squirrel-cage induction motors," *IEEE Trans. Ind. Appl.*, vols. IA–20, no. 1, pp. 46–55, Jan. 1984.

[9] M. Muchlas and H. Soetedjo, "Use of the maximum torque sensor to reduce the starting current in the induction motor," *Sensors Transducers*, vol. 114, no. 3, pp. 161–169, Mar. 2010.

[10] G. Zenginobuz, I. Cadirci, M. Ermis, and C. Barlak, "Performance optimization of induction motors during voltage-controlled soft starting," *IEEE Trans. Energy Convers.*, vol. 19, no. 2, pp. 278–288, Jun. 2004.

[11] K. Sundareswaran and P. S. Nayak, "Ant colony based feedback controller design for soft-starter fed induction motor drive," *Appl. Soft Comput.*, vol. 12, no. 5, pp. 1566–1573, May 2012.

[12] L. Rajaji, C. Kumar, and M. Vasudevan, "Fuzzy and ANFIS based soft starter fed induction motor drive for high performance applications," *ARPN J. Eng. Appl. Sci.*, vol. 3, no. 4, pp. 12–24, Aug. 2008.

[13] A. Gastli and M. M. Ahmed, "ANN-based soft starting of voltage-controlled-fed IM drive system," *IEEE Trans. Energy Convers.*, vol. 20, no. 3, pp. 497–503, Sep. 2005.

[14] S. Leng, A. R. N. M. R. Ul Haque, N. Perera, A. Knight, and J. Salmon, "Soft start and voltage control of induction motors using floating capacitor H-Bridge converters," *IEEE Trans. Ind. Appl.*, vol. 52, no. 4, pp. 3115–3123, Jul. 2016.

[15] T. Laczynski and A. Mertens, "Predictive stator current control for medium voltage drives with LC filters," *IEEE Trans. Power Electron.*, vol. 24, no. 11, pp. 2427–2435, Nov. 2009.

[16] S. Mukherjee and G. Poddar, "Fast control of filter for sensorless vector control SQIM drive with sinusoidal motor voltage," *IEEE Trans. Ind. Electron.*, vol. 54, no. 5, pp. 2435–2442, Oct. 2007.

[17] M. Swamy, J. Kang, and K. Shirabe, "Power loss, system efficiency and leakage current comparison between Si IGBT VFD and SiC FET VFD with various filtering options," *IEEE Trans. Ind. Appl*, vol. 51, no. 5, pp. 3858–3866, Sep./Oct. 2015.
[18] P. Mishra and R. Maheshwari, "Design, analysis, and impacts of sinusoidal LC filter on pulsewidth modulated inverter fed-induction motor drive," *IEEE Trans. Ind. Electron.*, vol. 67, no. 4, pp. 2678–2688, Apr. 2020.
[19] P. Mishra, R. Maheshwari, and D. Patil, "Stabilization of rotor flux-oriented control of induction motor with filter by active damping," *IEEE Trans. Ind. Electron.*, vol. 66, no. 12, pp. 9173–9183, Dec. 2019.
[20] H. Cai, L. Gao, and L. Xu, "Calculation of maximum torque operating conditions for inverter-fed induction machine using finite-element analysis," *IEEE Trans. Ind. Electron.*, vol. 66, no. 4, pp. 2649–2658, Apr. 2019.
[21] S. Madanzadeh, A. Abedini, A. Radan, and J.-S. Ro, "Application of quadratic linearization state feedback control with hysteresis reference reformer to improve the dynamic response of interior permanent magnet synchronous motors," *ISA Trans.*, vol. 99, pp. 167–190, Apr. 2020.
[22] K. Hatua, A. K. Jain, D. Banerjee, and V. T. Ranganathan, "Active damping of output *LC* filter resonance for vector-controlled VSI-fed AC motor drives," *IEEE Trans. Ind. Electron.*, vol. 59, no. 1, pp. 334–342, Jan. 2012.
[23] M. K. Metwaly, H. Z. Azazi, S. A. Deraz, M. E. Dessouki, and M. S. Zaky, "Power factor correction of three-phase PWM AC chopper fed induction motor drive system using HBCC technique," *IEEE Access*, vol. 7, pp. 43438–43452, 2019.
[24] M. M. Amin and O. A. Mohammed, "Development of high-performance grid-connected wind energy conversion system for optimum utilization of variable speed wind turbines," *IEEE Trans. Sustain. Energy*, vol. 2, no. 3, pp. 235–245, Jul. 2011.

SADJAD MADANZADEH (Graduate Student Member, IEEE) received the B.S. degree in electrical engineering from the University of Zanjan, Zanjan, Iran, in 2010, and the M.S. degree in electrical engineering from the K. N. Toosi University of Technology, Tehran, Iran, in 2013. He is currently a Researcher with Chung-Ang University, Seoul, South Korea. His research interests include electric drives control, electrical machine design, and power electronics.

SYED SABIR HUSSAIN BUKHARI (Member, IEEE) was born in Khairpur Mirs, Sindh, Pakistan, in 1986. He received the B.E. degree in electrical engineering from the Mehran University of Engineering and Technology, Jamshoro, Pakistan, in 2009, and the Ph.D. degree from the Department of Electronic Systems Engineering, Hanyang University, South Korea, in 2017. He joined Sukkur IBA University, in December 2016, as an Assistant Professor. He is currently working as a Research Professor with Chung-Ang University, Seoul, South Korea, under Korean Research Fellowship (KRF) Program. His main research interests include electric machine design, power quality, and drive controls.

JONG-SUK RO received the B.S. degree in mechanical engineering from Hanyang University, Seoul, South Korea, in 2001, and the Ph.D. degree in electrical engineering from Seoul National University (SNU), Seoul, in 2008. He conducted research at the Research and Development Center, Samsung Electronics, as a Senior Engineer, from 2008 to 2012. From 2012 to 2013, he was with the Brain Korea 21 Information Technology, SNU, as a Postdoctoral Fellow. He conducted research at the Electrical Energy Conversion System Research Division, Korea Electrical Engineering and Science Research Institute, as a Researcher, in 2013. From 2013 to 2016, he worked with the Brain Korea 21 Plus, SNU, as a BK Assistant Professor. In 2014, he was with the University of Bath, Bath, U.K. He is currently an Associate Professor with the School of Electrical and Electronics Engineering, Chung-Ang University, Seoul. His research interests include the analysis and optimal design of next-generation electrical machines using smart materials, such as electromagnet, piezoelectric, and magnetic shape memory alloy.